



Classification of Airborne Laser Bathymetry Data Using Artificial Neural Networks

Tomasz Kogut  and Adam Slowik 

Abstract—The current development of technology allows for extensive use of active remote sensing systems in water environment research. The data obtained using airborne bathymetric scanning are mainly used to build digital elevation models of the seabed. As a result, their information potential is largely untapped, because full-waveform data have considerably more information that can be used for classification with different machine learning algorithms. This article presents the process of classification and detection of objects on the seabed using multilayer perceptron neural networks. The features of full waveform and point cloud geometry were considered for network training. The results obtained allow for almost 100% correct classification of water surface and seabed. The seabed object points were also classified with an accuracy of over 80%. The obtained results increase the effectiveness of object detection compared to the other well-known classification algorithms.

Index Terms—Airborne laser bathymetry (ALB), classification, neural networks, obstacles, underwater objects detection.

I. INTRODUCTION

SEABED topography measurements are one of the main tasks of hydrographic organizations worldwide. The development of sea transport and the associated increase in ship traffic means that a great deal of attention is paid to ensuring safety through periodic monitoring of the seabed on ships' navigation routes. The occurrence of a possible catastrophe in maritime traffic may contaminate the environment for many years. Therefore, more and more attention is being paid to the development of more effective methods for detecting objects and monitoring possible obstacles along the transport route [1], [2].

Airborne laser bathymetry (ALB) is fast, and is a partial alternative method of measurement to echo sounding. There are the following two main types of bathymetric scanners: 1) with a green laser beam of 532 nm and 2) with two laser beams: green (532 nm) and infrared (1064 nm). In the perfect case, each green laser pulse should return an echo from the water surface and seabed. But in practice, it is not always so, because it depends on the water condition. The additional infrared beam cannot penetrate through the water column and it is used to provide

Manuscript received September 30, 2020; revised November 18, 2020 and December 9, 2020; accepted January 7, 2021. Date of publication January 12, 2021; date of current version January 29, 2021. (Corresponding author: Tomasz Kogut.)

The authors are with the Koszalin University of Technology, 75-453 Koszalin, Poland (e-mail: tomasz.kogut@tu.koszalin.pl; adam.slowik@tu.koszalin.pl).

Digital Object Identifier 10.1109/JSTARS.2021.3050799

information about the water surface, but does not guarantee that there is enough energy to be scattered back to the receiver [3].

The collected data are processed using appropriate algorithms that allow the information contained in these datasets to classify and detect objects [4], [5]. Attempts are being made to establish optimal conditions for ALB data acquisition and processing [6], however, there is a need for further research on the analysis of the full waveform of airborne bathymetric scanning and processing of the collected data [4]. The seabed return in an ALB waveform can provide the information about bottom morphology [7]–[10].

In the literature, authors have tested various machine learning techniques for their classification. Sun *et al.* [11] developed a hybrid algorithm for seabed sediment type classification. In the presented research experiment, they conducted a two-stage process of ALB data classification using the K -means and support vector machine (SVM) algorithms. Compared to the SVM algorithm itself, the use of K -means + SVM hybrid algorithm improved overall classification accuracy by 24%. Kumpumaki *et al.* [12] clustered the return pulses of bathymetric laser scanning based on the waveform shape. Similar shapes of the reflected waveform may correspond to different types of bottom coverage. A relatively sharp wave shape indicates, for example, a high probability of silt or clay in deeper waters. The authors used an algorithm of self-organizing networks to classify types of marine substrates. Eren *et al.* [13] used the SVM to differentiate between: 1) sand and rock bottoms and subsequently, 2) fine and coarse sand bottoms. They are based on waveform features obtained from the bottom return residual analysis. The classification results are 96% overall accuracy for sand and rock, and 86% overall accuracy for fine and coarse. Kogut *et al.* [14] used the random forest (RF) algorithm to classify point clouds from ALB, obtaining better results compared to SVM.

The aim of the study presented in this article is to classify and detect objects on the seabed in the point cloud obtained by ALB. To achieve the goal, multilayer perceptron (MLP) artificial neural networks (ANNs) with the softmax activation function were used, which allowed the examination of the probability of assigning objects to the appropriate class. The MLP neural network and other classification machine learning algorithms are very popular techniques and possess a very wide range of engineering applications (including in remote sensing) such as the integration of the spectral and spatial location features for water bathymetry [1], identification of surface water in Landsat 8 satellite images [15], automatic classification from high-resolution images [16], predicting species diversity of benthic communities within turbid nearshore using full-waveform

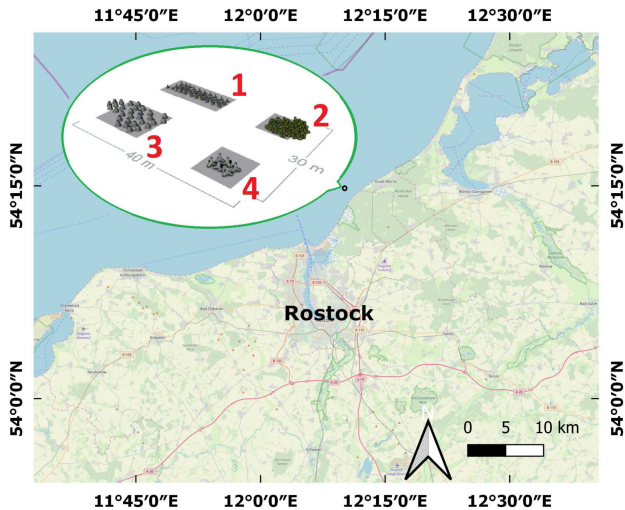


Fig. 1. Location of the test object.

ALB [17], benthic classifications using bathymetric LIDAR waveforms and integration of local spatial statistics and textural features [10].

The original contribution of this article can be summarized as follows.

- 1) An approach to the ALB point cloud classification using geometric and full-waveform features.
- 2) A description of the ANN with the softmax layer, which is applied to the determination of classification probability values of a given input point to each of the three output classes, respectively.

The rest of this article is organized as follows. Section II describes the test area and ALB data. Section III presents features description and the MLP neural network in detail. Section IV describes the results obtained using the proposed approach and some discussion. Finally, Section V concludes this article.

II. MATERIALS

A. Test Area

The test area is the artificial reef Rosenort on the Baltic Sea, located approximately 25 km north of the city of Rostock in Germany. The Rosenort reef is made up of four artificially created zones. The zones were built from the following:

- 1) fifty two-ton concrete tetrapods;
- 2) one hundred and eighty tons of stones;
- 3) thirty cut concrete cones;
- 4) six six-ton concrete tetrapods [18] (see Fig. 1).

The objects are located about 2 km from the shoreline at a depth of approximate 6 m.

B. ALB Data

The data were obtained in September 28–29, 2013 using an AHAB Chiroptera I scanner with a 400 m flight altitude, which is equipped with two beams (532 nm green and 1064 nm infrared) and scans with an elliptical shape with a deviation from the nadir by $\pm 20^\circ$ across and $\pm 14^\circ$ along the intended flight direction.

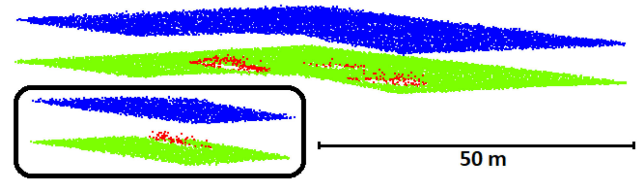


Fig. 2. Classified point cloud with detected objects at the seabed.

The horizontal nominal accuracy of the measurement is 0.75 m for the green beam and 0.2 m for the infrared beam, while the depth nominal accuracy is 0.15 m. The Secchi depth that can be achieved with the scanner is 1.5. During the measurement, the Secchi depth was about 6.3 m, which is close to the average value of Secchi depth for this region [19]. The secondary full-waveform analysis was used for data processing [20]. The first step of this approach is the Gaussian decomposition of a full waveform. After that were a large number of missing points of the seabed objects. Therefore, the beams with one peak need a second analysis. The preliminary location of a second echo in the full waveform with one peak was estimated based on the location of the second return in the neighboring full waveform with two peaks. To determine the exact position of the peak the search window was used with 30 samples before and after the approximated location. The last step of this approach is the Gaussian function fitting to the samples in the search window. After the calculations, 13 341 points were obtained on the water surface, 16714 points on the seabed, and 285 points on the seabed objects. In this research, we have analyzed the point cloud obtained from the green beam. The average point cloud density for the test object was 2.6 points/m² on the water surface and 3.3 points/m² on the seabed. The data used in the experimental portion of this article were obtained within the framework of the project, which is mentioned in the Acknowledgements section.

III. METHODOLOGY

The bathymetric dataset for training the ANN consisted of 6198 vectors (Fig. 2 data in the black box). A total of 80% of these vectors was used for the ANN training, and the remaining 20% was used for ANN validating during error back-propagation algorithm operation.

Each of the vectors contained 18 elements that described values of 15 input attributes (from U_1 to U_{15}) and 3 output classes (from U_{38} to U_{40}). These three classes were marked as follows: class 1: “water surface” (U_{38}) containing 2729 vectors, class 2: “seabed” (U_{39}) with 3396 vectors, and class 3: “seabed object” (U_{40}) represented by 73 vectors. Table I shows the numbering and description of attributes (ANN inputs) and classes (ANN outputs). Attributes can be divided into the following two groups of features: based on the full reflected wave (U_{1-5}) and resulting from the geometry of the point cloud (U_{6-15}) [21]–[23], which were calculated by analyzing the position of each point together with its neighborhood in a strictly determined region, defined by a cylinder with a radius $r = 5$ m (see Fig. 3: red color—analyzed point, purple color—radius (r) of cylinder, green color—points selected for analysis, gray color—other points).

TABLE I
DESCRIPTION OF ANN INPUTS AND OUTPUTS

U_i	Description	Formula
U_1	amplitude - describes the maximum value of the Gaussian curve and is closely related to the reflectance intensity [27]	—
U_2	echo width - (ω , full width at half maximum, FWHM) - it is the distance between two points on the Gaussian curve where the function takes half of its maximum value and can be defined in the Gaussian function σ based on standard deviation	$\omega = 2 * \sqrt{2 * \ln(2)} * \sigma$ (1)
U_3	return number (N)	—
U_4	number of returns (N_t)	—
U_5	normalized echo (N_z)	$N_z = \frac{N}{N_t}$ (2)
U_6	height difference (dz) - is defined as the difference of the Z coordinate between the analyzed point z_i and the lowest z_{min} in the analyzed area	$dz = z_i - z_{min}$ (3)
U_7	height variance (σ^2) - a feature that is a measure of variability. It is defined as the arithmetic mean of the squares of deviations of individual values z_i in the analyzed area from the mean value \bar{z}	$\sigma^2 = \frac{1}{n} \sum_{i=1}^n (z_i - \bar{z})^2$ (4)
U_8	eigenvalue λ_1	—
U_9	eigenvalue λ_2	—
U_{10}	eigenvalue λ_3	—
U_{11}	Sphericity - a feature describing the convexity or concavity of the position of a point relative to selected points	$S_\lambda = \frac{\lambda_3}{\lambda_1}$ (5)
U_{12}	Planarity - a feature representing the plane character of the arrangement of points	$P_\lambda = \frac{\lambda_2 - \lambda_3}{\lambda_1}$ (6)
U_{13}	Linearity - a feature showing the linear (continuous) character of the distribution of points	$L_\lambda = \frac{\lambda_1 - \lambda_2}{\lambda_1}$ (7)
U_{14}	Eigentropy - entropy calculated from own values	$E_\lambda = - \sum_{i=1}^3 \lambda_i \ln \lambda_i$ (8)
U_{15}	Omnivariance - a feature whose low values correspond to flat regions or linear structures, while high values are related to the spatial distribution of points [22]	$O_\lambda = \sqrt[3]{\prod_{i=1}^3 \lambda_i}$ (9)
U_{38}	Class 1: "water surface"	—
U_{39}	Class 2: "seabed"	—
U_{40}	Class 3: "seabed object"	—

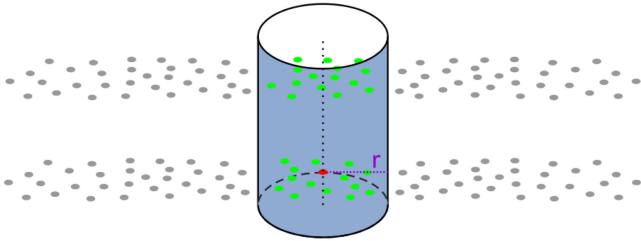


Fig. 3. Points in the area defined by cylinder with 5-m radius.

The objective of full-waveform processing is to obtain the most precise information on the location and characteristics of the object (target) based on the received signal, the quality of which depends, among others, on the emitted beam, the reflecting object (target), and the receiver.

For the purpose of training the ANN, the number of vectors in each class was made equal by a random down-sampling of vectors from class 1 and class 2 to the number of vectors in class 3. The dataset prepared in this way, consisting of three equal classes, consisted of $3 \times 73 = 219$ vectors. In a further stage of data processing, the data were normalized in accordance with the relationship

$$U_i^* = \frac{U_i - \text{mean}_i}{\text{stdev}_i} \quad (10)$$

where $i \in \{1, \dots, 15\}$, U_i^* —new value of attribute U_i after its normalization, mean_i —the mean value of all attribute values U_i , stdev_i —standard deviation of the attribute U_i .

The mean_i and stdev_i data characterizing the distribution of the i th attribute data were stored to use their values to normalize new data during the pattern recognition process by a trained ANN.

The architecture of the adopted ANN is MLP [24]–[26] and consists of 15 inputs and three outputs (see Fig. 4). It has three layers of neurons with full connections in each layer. The first (input) layer has 15 neurons, the second (intermediate) layer contains seven neurons, and the third (output) layer contains three neurons. Neurons in the first-two layers have a unipolar sigmoid activation function of the following form:

$$U_i = f(S_i) = \frac{1}{1 + e^{-S_i}} \quad (11)$$

where $i \in \{16, \dots, 37\}$, S_i —weighted sum determined by relationship

$$S_i = \sum_{k=x}^y (w_{i,k} \times U_k) \quad (12)$$

where $x = 1$ and $y = 15$ (for the first layer of neurons from U_{16} to U_{30}) or $x = 16$ and $y = 30$ (for the second layer of neurons

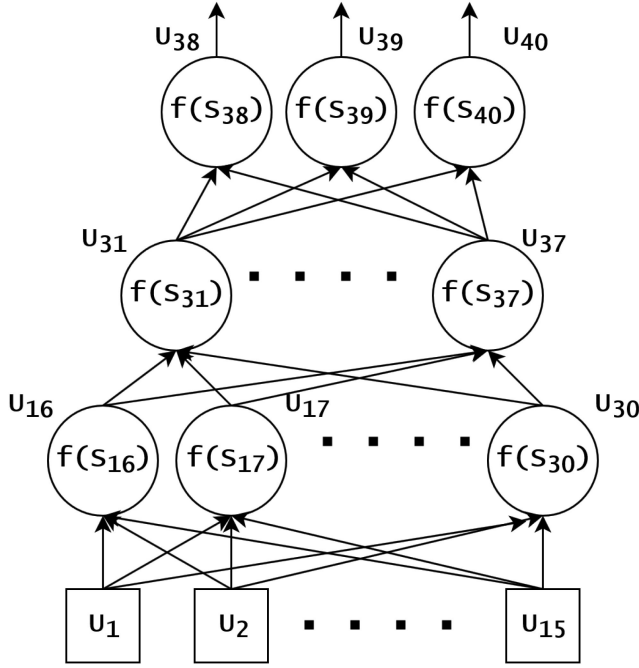


Fig. 4. ANN architecture.

from U_{31} to U_{37} , $w_{i,k}$ —the value of the weight that supply the signal to the i th neuron from the k th neuron output or from the k th input of an ANN, U_k —the value from the k th neuron output or from the k th input of an ANN.

Neurons in the third layer (from U_{38} to U_{40}) have a softmax activation function, which is described by the relationship

$$U_i = f(S_i) = \frac{e^{S_i}}{\sum_{i=38}^{40} f(S_i)} \quad (13)$$

where $i \in \{38, \dots, 40\}$, S_i —weighted sum calculated by relationship (12) and assuming the value $x = 31$ and $y = 37$. By using a softmax layer (from U_{38} to U_{40}) at the output of an ANN, the classification process results in probability values at the outputs of the ANN, which indicate the degree of belonging of a given input vector to each of the three classes. ANN from Fig. 4 was trained using an error back-propagation algorithm with a learning coefficient of $ro = 0.01$. The training algorithm was stopped after 1750 iterations. In each iteration, a randomly selected training vector (vector selected from a previously prepared set of $3 \times 73 = 219$ vectors) was given to the input of the ANN. Then, a forward-propagation phase was carried out, which consisted of determining the values of all the weighted sums S_i ($i \in \{16, \dots, 40\}$) and all the output values U_i ($i \in \{16, \dots, 40\}$). After the forward-propagation phase, the backward-propagation phase began, which consisted of determining the δ_i coefficient for each i th neuron.

For the neurons of the output layer ($i \in \{38, \dots, 40\}$), the δ_i coefficients were determined according to the relationship

$$\delta_i = (C_i - U_i) \times f'(S_i) \quad (14)$$

where C_i —the correct value at the U_i output resulting from the currently processed vector taken from the training set, U_i —the

TABLE II
CONFUSION MATRIX

Class	water surface		seabed		seabed object	
	(points)	(%)	(points)	(%)	(points)	(%)
water surface	10612	100	0	0	0	0
seabed	0	0	13119	98.5	199	1.5
seabed object	0	0	38	17.9	174	82.1

TABLE III
DESCRIPTION AND VALUE OF PARAMETER SETTINGS FOR
COMPARATIVE METHODS

Method	Parameter settings
SVM (Linear)	Kernel function: linear; Multiclass SVM
SVM (Quadratic)	Kernel function: quadratic; Multiclass SVM
SVM (Cubic)	Kernel function: cubic; Multiclass SVM
Random Forest	Number of trees: 30
Complex Tree	Split criterion: Gini index
RUSBoosted Trees	Number of trees: 30; Learning rate: 0.1
k-NN (k=1)	Number of neighbors: 1; Distance metric: Euclidean; Distance weight: equal
k-NN (k=3)	Number of neighbors: 3; Distance metric: Euclidean; Distance weight: equal
Weighted k-NN (k=3)	Number of neighbors: 3; Distance metric: Euclidean; Distance weight: squared inverse

value at the i th output of the ANN obtained after the forward-propagation phase, $f'(S_i)$ —value of the derivative activation function for the i th neuron.

For the neurons of the intermediate layer ($i \in \{31, \dots, 37\}$), and for the neurons of the input layer ($i \in \{16, \dots, 30\}$), the δ_i coefficients were determined according to the relationship

$$\delta_i = \left(\sum_{j=x}^y w_{j,i} \times \delta_j \right) \times f'(S_i) \quad (15)$$

where $x = 38$ and $y = 40$ (for the neurons of intermediate layer U_{31} to U_{37}) or $x = 31$ and $y = 37$ (for the neurons of the input layer U_{16} to U_{30}).

Once the δ_i values for all neurons were determined, all weight values were modified according to the relationship

$$w_{i,k}^* = w_{i,k} + ro \times \delta_i \times U_k \quad (16)$$

where $w_{i,k}^*$ —new weight $w_{i,k}$.

The weight update process completes the calculations related to the algorithm in a single iteration. Then, the algorithm goes to the next iteration and the whole process is repeated until the maximal number of iterations is reached. When the maximal number of iterations is reached the training algorithm stops.

IV. RESULTS AND DISCUSSION

The proposed approach was tested by conducting the training of MLP neural network (see Section III) 11 times. The error back-propagation algorithm is an algorithm with a random starting point. Therefore, for results to be meaningful, the training process had to be repeated several times.

After each training, the quality of the obtained neural classifier was tested on the basis of a set of 24142 vectors with the following distribution in particular classes: class 1: “water surface” (10612 vectors), class 2: “seabed” (13318 vectors), and class 3: “seabed object” (212 vectors). The class for which the

TABLE IV
CLASSIFICATION ACCURACY FOR DIFFERENT METHODS AND POINTS DISTRIBUTION FOR SEABED OBJECTS AFTER CLASSIFICATION (MANUAL CLASSIFICATION: OBJECT 2–79 POINTS, OBJECT 3–97 POINTS, OBJECT 4–36 POINTS)

Method	Classification accuracy (%)				Points distribution for seabed objects					
	overall	water surface	seabed	seabed object	object 2		object 3		object 4	
					(points)	(%)	(points)	(%)	(points)	(%)
Proposed MLP	93.53	100	98.51	82.08	78	98.73	72	74.23	24	66.67
SVM (Linear)	88.01	99.94	99.95	64.15	64	81.01	54	55.67	18	50
SVM (Quadratic)	86.44	99.97	99.92	59.43	65	82.28	46	47.42	15	41.67
SVM (Cubic)	85.77	100	99.77	57.55	70	88.61	38	39.18	14	38.89
Random Forest	85.99	100	99.94	58.02	66	83.54	50	51.55	7	19.44
Complex Tree	85.95	99.66	99.69	58.49	63	79.75	49	50.52	12	33.33
RUSBoosted Trees	93.28	99.66	99.51	80.66	74	93.67	71	73.20	26	72.22
k-NN (k=1)	85.57	100	99.65	57.08	62	78.48	52	53.61	7	19.44
k-NN (k=3)	84.03	100	99.74	52.36	66	83.54	41	42.27	4	11.11
Weighted k-NN (k=3)	84.33	100	99.70	53.30	66	83.54	43	44.33	4	11.11

TABLE V
AVERAGE CLASSIFICATION ACCURACY FOR DIFFERENT METHODS

Method	Classification accuracy (%)							
	overall		water surface		seabed		seabed object	
	Average	St. deviation	Average	St. deviation	Average	St. deviation	Average	St. deviation
Proposed MLP	92.07	1.14	99.99	0.02	98.57	0.34	77.66	3.56
SVM (Linear)	86.25	1.64	99.95	0.02	99.92	0.06	58.88	4.90
SVM (Quadratic)	75.68	6.68	99.95	0.01	99.87	0.09	27.23	20.09
SVM (Cubic)	77.41	8.36	99.96	0.03	99.49	0.63	32.76	25.61
Random Forest	84.37	1.22	100	0	99.93	0.04	53.17	3.68
Complex Tree	85.76	1.77	99.66	0	99.61	0.21	58.02	5.39
RUSBoosted Trees	90.55	3.28	99.69	0.10	99.61	0.18	72.34	10.09
k-NN (k=1)	77.55	6.43	100	0	99.30	0.32	33.36	19.00
k-NN (k=3)	76.89	5.74	100	0	99.44	0.27	31.00	17.13
Weighted k-NN (k=3)	76.78	6.04	100	0	99.40	0.28	30.93	17.87

highest probability was obtained at the output of the ANN was chosen. Results were compared to manual classification. The overall classification accuracy (Acc_{ov} [%]) was computed using following equation:

$$Acc_{ov} = \frac{Acc_{water} + Acc_{seabed} + Acc_{seabedobject}}{3} \quad (17)$$

$$Acc_{water} = \left(\frac{Input_{water}}{Vectors_{water}} \right) \cdot 100\% \quad (18)$$

$$Acc_{seabed} = \left(\frac{Input_{seabed}}{Vectors_{seabed}} \right) \cdot 100\% \quad (19)$$

$$Acc_{seabedobject} = \left(\frac{Input_{seabedobject}}{Vectors_{seabedobject}} \right) \cdot 100\% \quad (20)$$

where Acc_{water} —the classification accuracy for class 1: “water surface,” Acc_{seabed} —the classification accuracy for class 2: “seabed,” $Acc_{seabedobject}$ —the classification accuracy for class 3: “seabed object,” $Input_{water}$ —the number of input vectors correctly classified to class 1: “water surface,” $Input_{seabed}$ —the number of input vectors correctly classified to class 2: “seabed,” $Input_{seabedobject}$ —the number of input vectors correctly classified to class 3: “seabed object,” $Vectors_{water}$ —the number of all vectors belonging to class 1: “water surface” in testing dataset ($Vectors_{water} = 10612$), $Vectors_{seabed}$ —the number of all vectors belonging to class 2: “seabed” in testing dataset ($Vectors_{seabed} = 13318$), $Vectors_{seabedobject}$ —the number of all vectors belonging to class 3: “seabed object” in testing dataset ($Vectors_{seabedobject} = 212$).

The conducted tests reached 100% correctness for the class “water surface.” For the “seabed,” this result ranged between 99.3% and 98%, while for the “seabed object” class, it ranged between 84.9% and 72.6%. Table II shows the results of the classification obtained using the proposed MLP neural network (we have chosen the neural network having the median of accuracy value from 11 training repetitions) in the form of an error matrix, where the result of “seabed objects” detection remains high at 82.1%.

The ANN significantly improves the classification of seabed object points and this directly affects the detection of objects, which was the purpose of this study. The applied softmax layer allows determining for a given point, the probability values of its belonging to the particular classes (“water surface,” “seabed,” and “seabed object”).

In Table IV, we have presented the classification accuracy comparison between the proposed MLP approach and other methods. The comparative methods were running with their default parameter values and were implemented using MATLAB 2019b Classification Learner tool. The description and value of parameters settings for the comparative methods are presented in Table III.

As we can see (from Table IV) the results obtained by the proposed method are better or comparable to the results obtained using other methods. Additionally, in relation to Fig. 1, the distribution of points for individual objects is presented. The object number 1 was not included in the list, because it was included in the training data. The proposed MLP approach has the best results on the objects 2 and 3. On the object 4 closest to the reference data is the RUSBoosted Trees method.

TABLE VI
 VALUES OF *t*-STUDENT TEST AND STATISTICAL IMPORTANCE EVALUATION OF DIFFERENCES BETWEEN THE ACCURACY RESULTS OBTAINED USING THE PROPOSED MLP AND THOSE OBTAINED USING THE OTHER METHODS FOR DIFFERENT SIGNIFICATION LEVEL (SIG. LEVEL): $\alpha = 0.01$, $\beta = 0.05$, AND $\gamma = 0.10$
 (“√”—RESULT IS STATISTICALLY SIGNIFICANT; “×”—RESULT IS NOT STATISTICALLY SIGNIFICANT)

Method	Statistical signification															
	overall			water surface			seabed			seabed object						
	t-value	sig. level		t-value	sig. level		t-level	sig. level		t-level	sig. level					
	α	β	γ		α	β	γ		α	β	γ		α	β	γ	
SVM (Linear)	9.67	✓	✓	✓	4.44	✓	✓	✓	-12.91	✓	✓	✓	10.29	✓	✓	✓
SVM (Quadratic)	8.02	✓	✓	✓	4.72	✓	✓	✓	-13.40	✓	✓	✓	8.20	✓	✓	✓
SVM (Cubic)	5.76	✓	✓	✓	2.22	×	✓	✓	-4.30	✓	✓	✓	10.09	✓	✓	✓
Random Forest	15.28	✓	✓	✓	-1.84	×	×	✓	-13.16	✓	✓	✓	15.87	✓	✓	✓
Complex Trees	9.33	✓	✓	✓	46.71	✓	✓	✓	-8.57	✓	✓	✓	5.76	✓	✓	✓
RUSBoosted Trees	1.45	×	×	×	9.35	✓	✓	✓	-9.28	✓	✓	✓	1.65	×	×	×
k-NN (k=1)	7.38	✓	✓	✓	-1.84	×	×	✓	-5.20	✓	✓	✓	7.60	✓	✓	✓
k-NN (k=3)	8.60	✓	✓	✓	-1.84	×	×	✓	-6.70	✓	✓	✓	8.85	✓	✓	✓
Weighted k-NN (k=3)	8.26	✓	✓	✓	-1.84	×	×	✓	-6.26	✓	✓	✓	8.51	✓	✓	✓

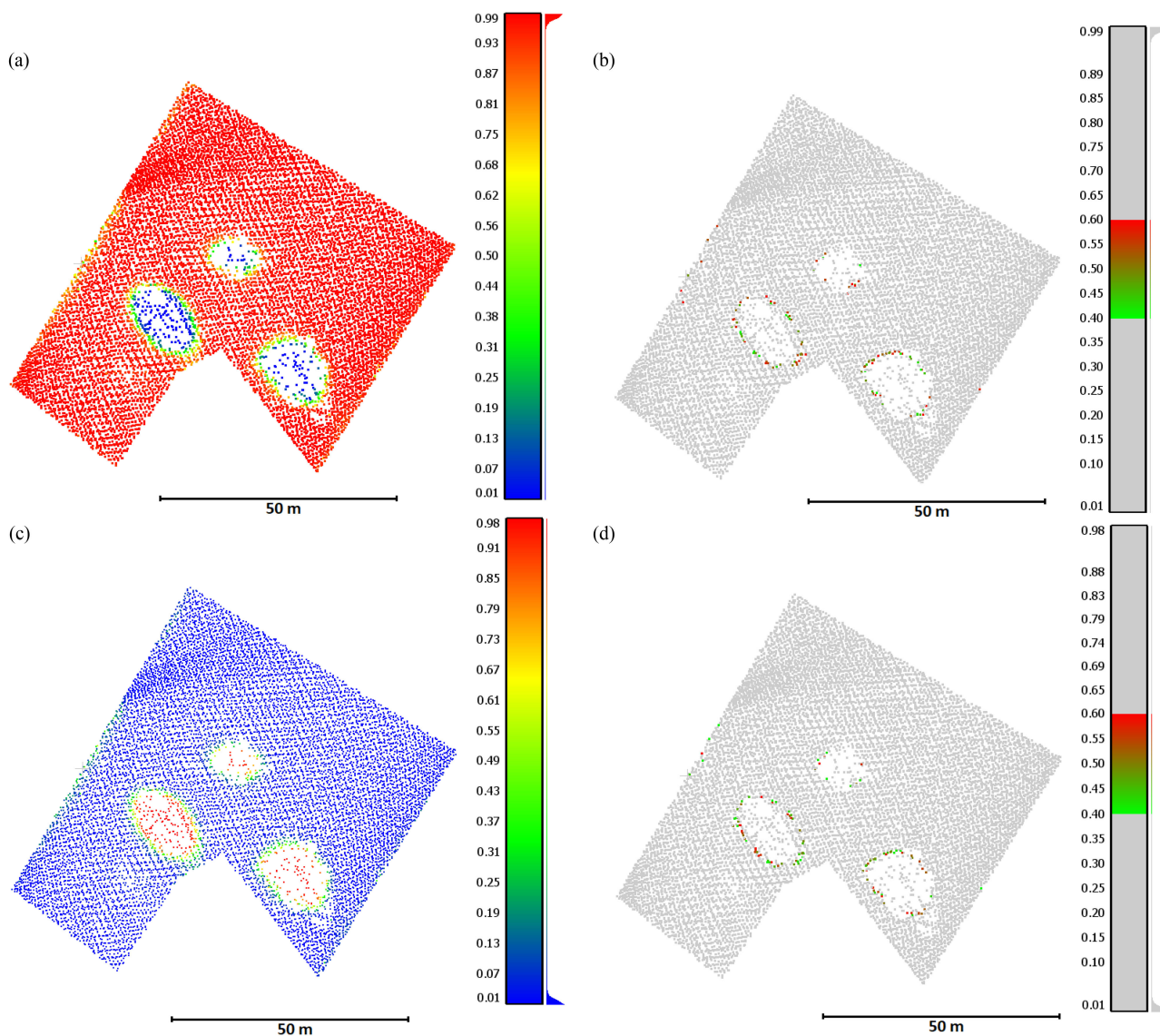


Fig. 5. Probability distribution for seabed class (A) and seabed object class (C). B and D represent probability in the range [0.4–0.6].

For better presentation of the results obtained using the proposed method and other comparative methods, the average values (Average) and standard deviation values (St. deviation) were presented in Table V. Each result was obtained after 11-fold repetition of each method. We can see that result obtained using the proposed MLP method is better or comparable to the results obtained using other methods.

In order to check the statistical importance of the results obtained using the proposed method, the t -Student statistical test was performed (see Table VI). The hypotheses on the equality of average values is true: with a trust level of 99% ($\alpha = 0.01$) when the absolute value of t -value is lower than 3.11, with a trust level of 95% ($\beta = 0.05$) when the absolute value of t -value is lower than 2.20, and with a trust level of 90% ($\gamma = 0.10$) when the absolute value of t -value is lower than 1.80.

Based on the t -Student test values (t -values), we can see that in terms of overall accuracy, for all but one of the other methods tested and all significance levels tested, the differences are statistically significant. However, when comparing the proposed MLP method's overall accuracy assessment results against those of RUSBoosted Trees, the differences are not statistically significant. When this analysis is extended to the individual classes (water surface, seabed, and seabed object), for the water surface classification, the differences between methods were, in several cases, not statistically significant, but this is due to the fact that every algorithm tested performed very well in classifying the water surface. In terms of seabed classification, the proposed MLP method actually did a bit worse than the others, and the differences were all statistically significant. However, since all of the seabed classification accuracies were $>98.5\%$, it can be said that all methods performed well. The seabed object classification was the most challenging and this was where the proposed MLP method was shown to outperform the others, again with the exception of RUSBoosted Trees, for which there was no statistically significant difference in the results from the proposed MLP algorithm.

In Fig. 5, we have analyzed these points for which the final decision about the classification is not clear. In this case, these are only points from the classes 2 and 3 for which the probability values for belonging to the given class are from the range 0.4–0.6. Within this range, 70% of points in class 2 were correctly classified to the “seabed.” In the class of “seabed objects” in the same range, about 50% of points are correctly classified. From the obtained results, it can be observed that the points on the border of the “seabed object” and the “seabed” have the least certainty of classification.

V. CONCLUSION

The MLP neural network was used in the study to classify airborne bathymetric scanning data to detect objects at the seabed. The classifications show that the selected features classify the point cloud well and allow the detection of objects on the seabed with an accuracy of about 80%. The results obtained significantly increase the effectiveness of object detection in relation to the most comparative algorithms. Additional probability analysis allows for further assessment of points whose classification certainty is low.

ACKNOWLEDGMENT

The authors would like to thank the Institute of Photogrammetry and GeoInformation in Hannover and BSH Rostock for the data used in this article.

REFERENCES

- [1] Y. Wang, X. Zhou, C. Li, Y. Chen, and L. Yang, “Bathymetry model based on spectral and spatial multifeatures of remote sensing image,” *IEEE Geosci. Remote Sens. Lett.*, vol. 17, no. 1, pp. 37–41, Jan. 2020.
- [2] Z. Pan, C. L. Glennie, J. C. Fernandez-Diaz, C. J. Legleiter, and B. Overstreet, “Fusion of LiDAR orthowaveforms and hyperspectral imagery for shallow river bathymetry and turbidity estimation,” *IEEE Trans. Geosci. Remote Sens.*, vol. 54, no. 7, pp. 4165–4177, Jul. 2016.
- [3] G. Mandlbürger, M. Pfennigbauer, and N. Pfeifer, “Analyzing near water surface penetration in laser bathymetry—A case study at the river Pielach,” *ISPRS Ann. Photogrammetry Remote Sens. Spatial Inf. Sci.*, vol. II-5/W2, pp. 175–180, 2013.
- [4] C. Wang, Q. Li, Y. Liu, G. Wu, P. Liu, and X. Ding, “A comparison of waveform processing algorithms for single-wavelength LiDAR bathymetry,” *J. Photogrammetry Remote Sens.*, vol. 101, pp. 22–35, 2015.
- [5] K. Ding *et al.*, “An improved quadrilateral fitting algorithm for the water column contribution in airborne bathymetric lidar waveforms,” *Sensors*, vol. 18, no. 2, 2018, Art. no. 552.
- [6] K. Richter, G.-H. Maas, P. Westfeld, and R. Weis, “An approach to determining turbidity and correcting for signal attenuation in airborne lidar bathymetry,” *J. Photogrammetry, Remote Sens. Geoinformation Sci.*, vol. 85, no. 1, pp. 31–40, 2017.
- [7] A. Collin, P. Archambault, and B. Long, “Mapping the shallow water seabed habitat with the SHOALS,” *IEEE Trans. Geosci. Remote Sens.*, vol. 46, pp. 2947–2955, Oct. 2008.
- [8] H. M. Tulldahl and S. A. Wikstrom, “Classification of aquatic macrovegetation and substrates with airborne lidar,” *Remote Sens. Environ.*, vol. 121, pp. 347–357, 2012.
- [9] H. M. Tulldahl, C. Vahlberg, A. Axelsson, H. Karlsson, and P. Jonsson, “Sea floor classification from airborne lidar data,” *Proc. SPIE*, vol. 6750, 2007, Art. no. 675003, doi: 10.1117/12.737922.
- [10] A. Collin, B. Long, and P. Archambault, “Benthic classifications using bathymetric LIDAR waveforms and integration of local spatial statistics and textural features,” *J. Coastal Res.*, vol. 62, pp. 86–98, 2011.
- [11] Y. D. Sun and S. W. Shyue, “A hybrid seabed classification method using airborne laser bathymetric data,” *J. Mar. Sci. Technol.*, vol. 25, no. 3, pp. 358–364, 2017.
- [12] T. Kumpumaki, P. Ruusuvaara, V. Kangasniemi, and T. Lipping, “Data-driven approach to benthic cover type classification using bathymetric LiDAR waveform analysis,” *Remote Sens.*, vol. 7, no. 10, pp. 13390–13409, 2015.
- [13] F. Eren, S. Peeri, Y. Rzhanov, and L. Ward, “Bottom characterization by using airborne lidar bathymetry (ALB) waveform features obtained from bottom return residual analysis,” *Remote Sens. Environ.*, vol. 206, pp. 260–274, 2018.
- [14] T. Kogut and M. Weistock, “Classifying airborne bathymetry data using the random forest algorithm,” *Remote Sens. Lett.*, vol. 10, no. 9, pp. 874–882, 2019.
- [15] W. Jiang *et al.*, “Multilayer perceptron neural network for surface water extraction in Landsat 8 OLI satellite images,” *Remote Sens.*, vol. 10, no. 5, 2018, Art. no. 755.
- [16] F. Del Frate, F. Pacifici, G. Schiavon, and C. Solimini, “Use of neural networks for automatic classification from high-resolution images,” *IEEE Trans. Geosci. Remote Sens.*, vol. 45, no. 4, pp. 800–809, Apr. 2007.
- [17] A. Collin, P. Archambault, and B. Long, “Predicting species diversity of benthic communities within turbid nearshore using full-waveform bathymetric LiDAR and machine learners,” *PLoS One*, vol. 6, no. 6, 2011, Art. no. e 21265.
- [18] Jul. 6, 2020. [Online]. Available: https://www.riff-nienhagen.de/riff_rosenort.shtml
- [19] T. Aarup, “Transparency of the North Sea and Baltic Sea—A Secchi depth data mining study,” *Oceanologia*, vol. 44, no. 3, pp. 323–337, 2002.
- [20] T. Kogut and K. Bakula, “Improvement of full waveform airborne laser bathymetry data processing based on waves of neighborhood points,” *Remote Sens.*, vol. 11, no. 10, 2019, Art. no. 1255.
- [21] H. Gross, U. Thoennessen, “Extraction of lines from laser point clouds,” *Fraunhofer FOM*, vol. 36, pp. 87–91, 2006.

- [22] J. Niemeyer, F. Rottensteiner, and U. Soergel, "Contextual classification of lidar data and building object detection in urban areas," *ISPRS J. Photogrammetry Remote Sens.*, vol. 87, pp. 152–165, 2014.
- [23] C. Nesrine, L. Guo, and C. Mallet, "Airborne lidar feature selection for urban classification using random forests," in *Proc. ISPRS Workshop: Laserscanning*, 2009, pp. 207–212.
- [24] R. Lippmann, "An introduction to computing with neural nets," *IEEE ASSP Mag.*, vol. 4, no. 2, pp. 4–22, Apr. 1987.
- [25] J. M. Zurada, *Introduction to Artificial Neural Systems*. Eagan, MN, USA: West Pub., 1992.
- [26] K. Shibata and Y. Ikeda, "Effect of number of hidden neurons on learning in large-scale layered neural networks," in *Proc. Int. Joint Conf.*, 2009, pp. 5008–5013.
- [27] W. Wagner, M. Hollaus, C. Briese, V. Ducic, "3D vegetation mapping using small-footprint full-waveform airborne laser scanners," *Int. J. Remote Sens.*, vol. 29, no. 5, pp. 1433–1452, 2008.



Tomasz Kogut was born in 1985. He received the B.S. degree in geodesy from Koszalin University of Technology, Koszalin, Poland, in 2008, and the M.E. degree in geodesy and geoinformatics from University of Applied Sciences in Neubrandenburg, Neubrandenburg, Germany, in 2011, and the Ph.D. degree in geodesy and cartography from Warsaw University of Technology, Warsaw, Poland, in 2017.

Since 2011, he has been with the Department of Geoinformatics, Koszalin University of Technology, Koszalin, Poland. His research interests include clas-

sification, lidar, lidar bathymetry, image analysis, and machine learning.

Dr. Kogut is a member of Polish Society for Photogrammetry and Remote Sensing and German Society for Photogrammetry, Remote Sensing, and Geoinformation.



Adam Slowik (Senior Member, IEEE) received the B.Sc. and M.Sc. degrees in computer engineering and electronics from Koszalin University of Technology, Koszalin, Poland, in 2001 and the Ph.D. degree with distinction, in 2007 from the Department of Electronics and Computer Science, Koszalin University of Technology, Koszalin, Poland, and the Dr. habil. degree in computer science (intelligent systems), in 2013 from the Department of Mechanical Engineering and Computer Science, Czestochowa University of Technology, Czestochowa, Poland.

Since October 2013, he has been an Associate Professor with the Department of Electronics and Computer Science, Koszalin University of Technology. His research interests include soft computing, computational intelligence, and, particularly, bioinspired optimization algorithms, and their engineering applications.

Dr. Slowik is a Reviewer for many international scientific journals. He is an author or coauthor of more than 100 refereed articles in international journals, two books, and conference proceedings, including one invited talk. He is currently an Associate Editor for the IEEE TRANSACTIONS ON INDUSTRIAL INFORMATICS. He is a member of the program committees of several important international conferences in the area of artificial intelligence and evolutionary computation. He was a recipient of one Best Paper Award (IEEE Conference on Human System Interaction—HSI 2008).